

1

2 **Deep Short-term Slow Slip and Tremor in the Manawatu Region, New Zealand**

3 **Shannon L. Fasola<sup>1</sup>, Noel M. Jackson<sup>1</sup>, and Charles A. Williams<sup>2</sup>**

4 <sup>1</sup>Department of Geology, University of Kansas, Lawrence, KS.

5 <sup>2</sup>GNS Science, Lower Hutt, New Zealand.

6 Corresponding author: Shannon Fasola ([shannon.fasola@ku.edu](mailto:shannon.fasola@ku.edu))

7 **Key Points:**

- 8
- GNSS data indicates newly detected short-term slow slip in region of deep tremor
  - 9 • Long-term slow slip events may influence these small slow slip events by increasing slip  
10 rates
  - 11 • Three types of slow slip overlap along-strike in Hikurangi margin: shallow, short-term;  
12 deep, long-term; deeper, short-term with tremor

## 13 **Abstract**

14 The Manawatu region experiences deep tremor and long-term SSEs; however tremor is adjacent  
15 to, and not co-located with, long-term SSEs. Observations of Episodic tremor and Slip (ETS)  
16 elsewhere suggest it is possible smaller short-term SSEs below the current detection threshold  
17 occur where tremor is observed. Therefore, we sought to determine if small SSEs occurred with  
18 Manawau tremor. We decomposed GNSS data using times of tremor to assess average surface  
19 displacements and performed a static slip inversion to model the displacement during tremor.  
20 The slip inversion suggested small slow slip partially coincided with tremor and long-term SSEs  
21 may influence these small SSEs by increasing slip rates. We suggest that the interface below  
22 deep long-term SSEs may slip often, in small ETS-like SSEs that are not individually detectable  
23 geodetically. The question remains as to the nature of the strong variability in SSE behavior with  
24 depth and duration in the southern Hikauangi margin.

## 25 **Plain Language Summary**

26 In between the Earth's tectonic plates, energy builds over time and can be released along faults  
27 suddenly (seconds-minutes; i.e., earthquakes) or slowly (weeks-years; i.e., slow slip events).  
28 Slow slip often happens with low-frequency earthquakes (i.e., tectonic tremor). The North  
29 Island, New Zealand features two colliding tectonic plates with the potential to generate large  
30 earthquakes. The interface between these plates has both deep tectonic tremor and large, long-  
31 lasting slow slip, but the tectonic tremor is deeper on the fault than the large slow slip. Studies  
32 have suggested small, short-lasting slow slip, usually not able to be detected, occur  
33 where tectonic tremor is found. In this study we tried a different approach to find the small slow  
34 slip. While small slow slip are not detected by themselves, we were able to detect their  
35 cumulative effect in the tectonic tremor area. We modeled small slow slip during tectonic tremor  
36 to find the mean sliding rate on the fault that is between the tectonic plates. The large long-  
37 lasting slow slip may drive these smaller slow slip by making them slip faster. The question  
38 remains as to the cause of the many types of slow slip in New Zealand.

## 39 **1 Introduction**

40 Tectonic tremor was first detected in the Nankai subduction zone in southwest Japan  
41 (Obara, 2002) and has since been discovered in several subduction zones around the world.

42 Tectonic tremor consists of low-level seismic vibrations representing a swarm of low-frequency  
43 earthquakes (Brown et al., 2009; Ide et al., 2007; Shelly et al., 2006, 2007). Tremor is often  
44 accompanied by and thought to be the result of slow slip events (SSEs; Bartlow et al., 2011;  
45 Shelly et al., 2006; Wech & Creager, 2007). As a result, tremor is thought to be a proxy for slow  
46 slip, and hence can be used to track and better understand SSEs. These aseismic ruptures occur  
47 on the plate interface in the frictional transition zone from stick-slip to stable sliding (Beroza &  
48 Ide, 2011; Dragert et al., 2001) or in zones of high pore fluid pressure and low effective stress  
49 (e.g. Gao & Wang, 2017; Hyndman et al., 2015). While the amount of strain released from  
50 tremor is relatively small, SSEs are capable of releasing as much strain along the plate interface  
51 as M 7+ earthquakes (e.g., Radiguet et al., 2012). There have also been cases where SSEs have  
52 been found to precede large megathrust earthquakes (e.g., Graham et al., 2014; Kato et al., 2012;  
53 Ruiz et al., 2014). Therefore, understanding the behavior of slow slip and tremor is valuable for  
54 estimating its potential impact on the seismic budget (e.g., Obara & Kato, 2016; Radiguet et al.,  
55 2016) and potential for triggering future earthquakes.

56 There are a variety of scenarios in which tremor occurs with slow slip. Tremor that  
57 spatiotemporally correlates with short-term SSEs is referred to as “episodic tremor and slip”  
58 (ETS) which is prominent in the Nankai and Cascadia subduction zones at depths of 25–45 km  
59 (Obara et al., 2004; Rogers & Dragert, 2003). Tremor is not always co-located with SSEs, but is  
60 instead found offset downdip from the region of slow slip as in the Bungo Channel in Japan and  
61 Costa Rica (Brown et al., 2009; Hirose et al., 2010). Bursts of tremor co-located with or near the  
62 down-dip limit of long-term SSEs have also been detected in Mexico, Alaska, and Japan, with a  
63 higher frequency of tremors during long-term SSEs (Frank et al., 2018; Hirose et al., 2010;  
64 Rousset et al., 2019). Frank et al. (2018) and Rousset et al. (2019) both suggested that long-term  
65 SSEs were actually composed of a cluster of short ETS-like events while Rousset et al. (2019)  
66 also proposed the long-term SSE may have occurred updip from a cluster of short ETS-like  
67 events. The difference in the variability in tremor behavior within and between subduction zones  
68 is not well understood. Therefore, it is important to study tremor and slow slip in as many  
69 regions as possible to evaluate the full range of behaviors.

70 The North Island of New Zealand along the Hikurangi margin provides an excellent  
71 opportunity to further investigate the wide range of tremor and slow slip behaviors. New Zealand  
72 has both shallow, short-term SSEs and deep, mid- to long-term SSEs. See Wallace (2020) for a



86 deep SSEs near Manawatu (Romanet & Ide, 2019). However, most SSEs in New Zealand are not  
87 accompanied by observed tectonic tremor. Instead, increased rates of seismicity are more  
88 commonly associated with SSEs at the Hikurangi margin (e.g., Bartlow et al. 2014; Delahaye et  
89 al. 2009; Jacobs et al. 2016; Reyners & Bannister 2007; Shaddock & Schwartz 2019; Yarce et al.  
90 2019). Wallace (2020) suggested the difference in the more dominant seismic signature could  
91 reflect the thermal structure of the subduction zone (Yabe et al., 2014), frictional heterogeneities  
92 in the region of slow slip (Wallace, Barnes, et al. 2012), and attenuation within the upper plate  
93 that would impact the ability of tremor to be recorded at the surface (Todd & Schwartz, 2016).

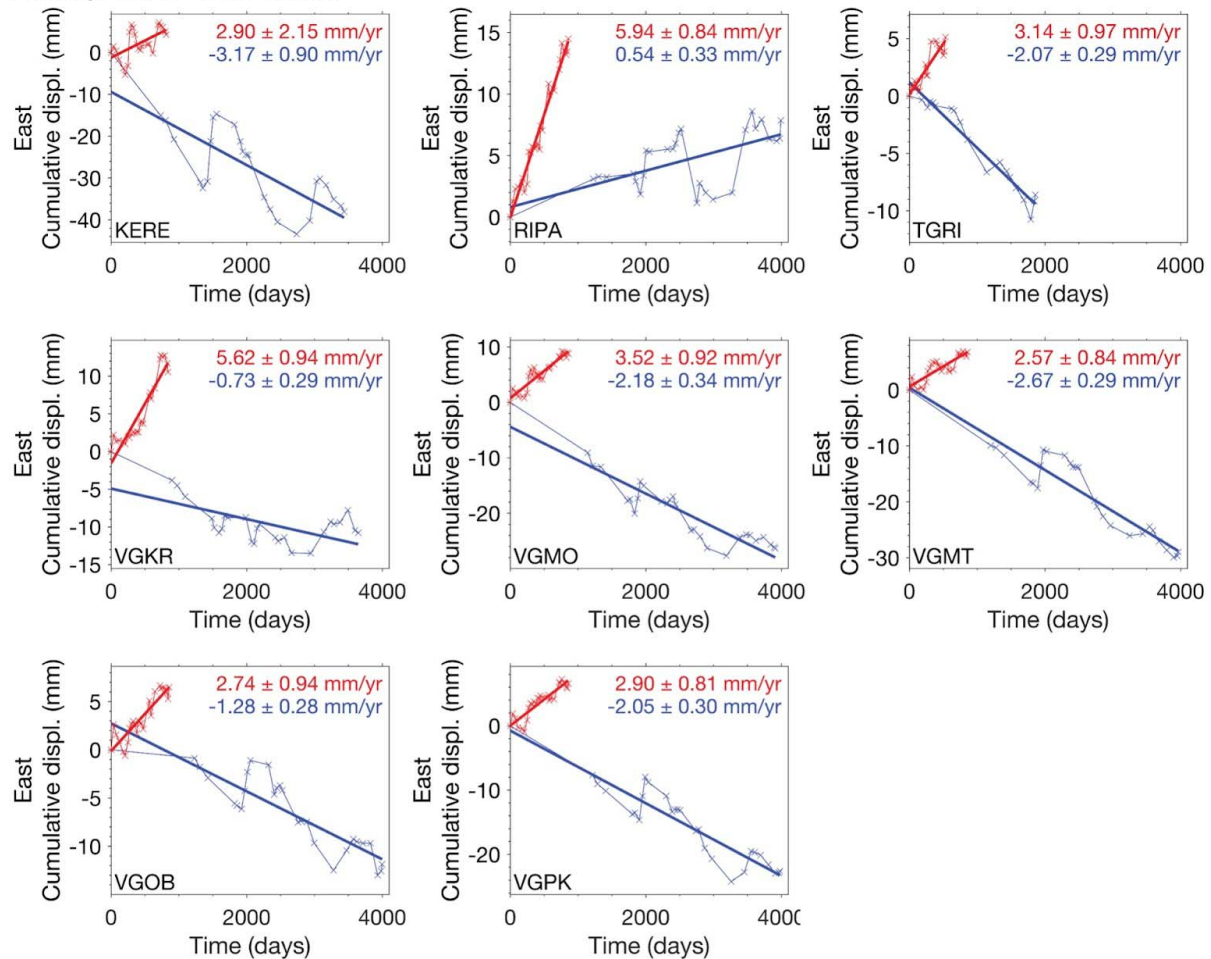
94 In this study, we focused on the deep portion of the central Hikurangi margin where large  
95 ( $M_w$  6.9-7.2), long-term (1-2 year) Manawatu SSEs and small ( $M_w$  6.6), mid-term (couple  
96 months) Kaimanawa SSEs occur at similar depth but are adjacent to each other along-strike  
97 (Figure 1) (Wallace, 2020). Tremor occurs down dip from the Manawatu and Kaimanawa SSEs  
98 and both during and in between times of SSEs (Romanet & Ide, 2019). Observations of ETS  
99 elsewhere in the world and more frequent tremor episodes relative to the mid- to long-term deep  
100 SSEs at the Hikurangi margin suggest it is possible smaller short-term SSEs below the current  
101 geodetic network detection threshold also occur in the area of observed tremor. This would  
102 indicate SSEs occur at three different depth ranges in the central Hikurangi margin. Therefore,  
103 we sought to further investigate tremor in the Manawatu region to determine if a detectable  
104 geodetic signal can be identified with decomposition, in which we stacked tremor displacement  
105 offsets on GNSS time series and calculated a time-averaged displacement rate. Time-averaged  
106 displacement rates during tremor periods were then compared with displacement rates outside of  
107 tremor periods and inverted to obtain a model of slip rate on the plate interface associated with  
108 tremor. It is valuable to understand how much of the seismic budget is being released  
109 aseismically and to what degree, if any, do the different types of SSEs impact each other. This  
110 study seeks to build on the understanding of the already complex nature of SSEs and tremor at  
111 the Hikurangi margin.

## 112 **2 Data and Methods**

113 For this study we used daily time-series solutions from continuous GNSS stations from  
114 the GeoNet network on the North Island (GNS Science, 2000). GNSS time series were  
115 referenced to the fixed Australian plate, and outliers and offsets due to antenna changes and

116 earthquakes were removed. Time series were regionally filtered by removing a common mode  
 117 signal (Figure S1). See supporting information for more details on post-processing of the time  
 118 series.

### Decomposition for All Tremor



119  
 120 **Figure 2.** Decomposition of the East components of the entire time series for stations whose  
 121 decompositions were found to be robust. Red and blue curves indicate cumulative offsets during  
 122 tremor and inter-tremor periods, respectively. Values represent velocities from a best-fit line and  
 123  $1\sigma$  uncertainties obtained from random resampling. See Figure S3 for east and north components  
 124 for all stations used in the inversion.

125 We decomposed the GNSS time series in the Manawatu region based on times of tremor  
 126 following the methods of Rousset et al. (2019). We used the tremor catalog from Romanet and  
 127 Ide (2019) which spans from 2005 through 2016 and consists of 354 events in the Manawatu

128 region. Therefore, time series used for decomposition ranged from 2005, or the start of station  
129 recording, until the day before the 14 November 2016  $M_w$  7.8 Kaikoura earthquake in order to  
130 avoid signals from the earthquake. Twelve GNSS stations surrounding the Manawatu tremor  
131 were used for decomposition which had no large gaps in data and were recording for at least two  
132 deep, mid- to long-term SSEs. We acknowledge that there are stations near the tremor that were  
133 not used for decomposition (Figure S1d). It is important to note that part of this region overlaps  
134 with the Taupo volcanic zone and there are multiple stations directly on volcanoes. Thus, we  
135 sought to limit the use of volcanic stations to avoid any volcanic signals.

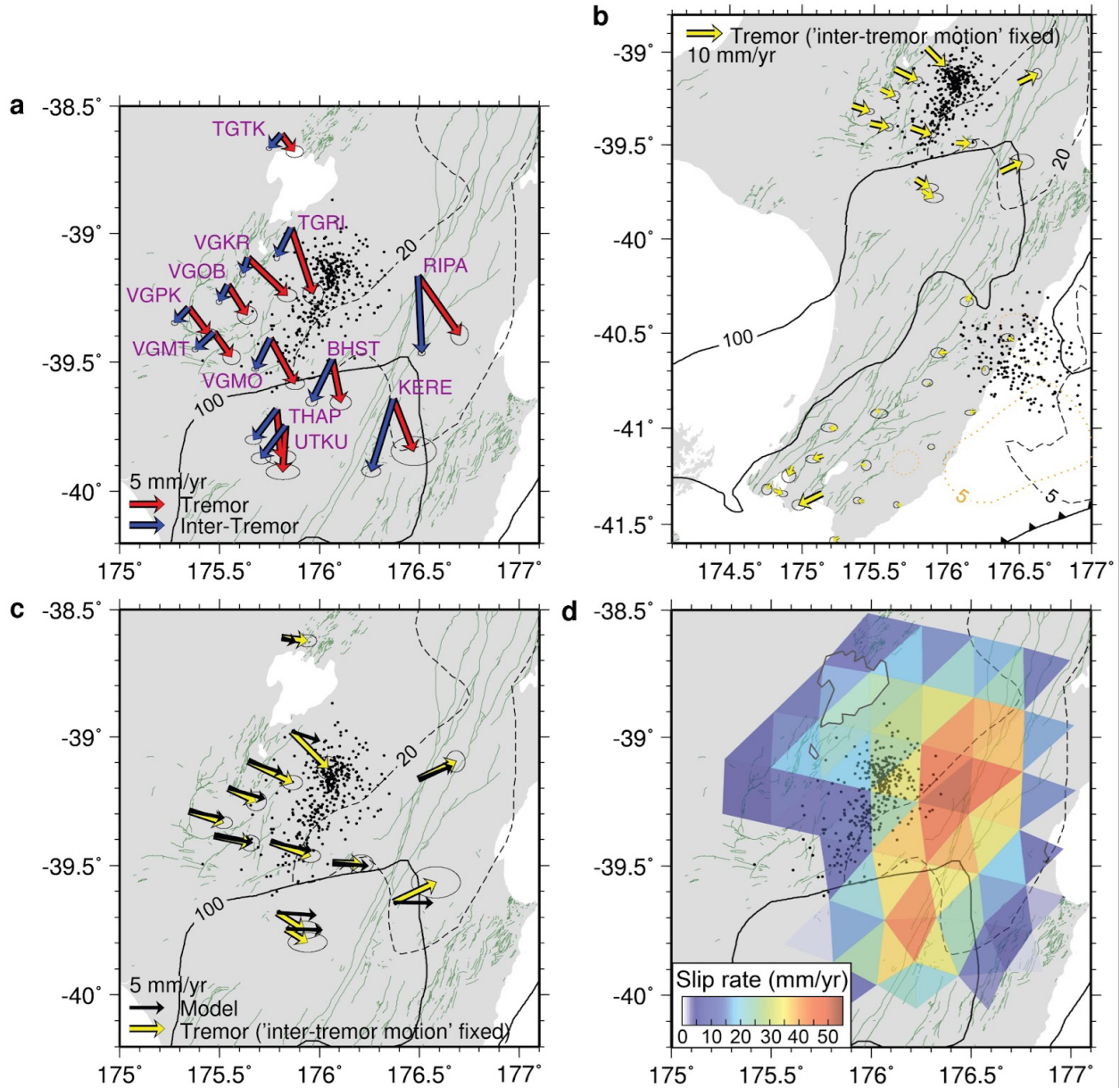
136 Tremor was grouped into clusters to identify bursts of tremor which are believed to  
137 represent transient slip (Frank et al., 2018; Hawthorne & Rubin, 2013; Villafuerte & Cruz-  
138 Atienza, 2017). As in Rousset et al. (2019), we used daily counts of tremor detections and  
139 grouped them into clusters based on a 22-day minimum inter-cluster duration and minimum  
140 number of 5 events per cluster (Figure S2). Due to the smaller tremor catalog relative to those in  
141 other studies applying the decomposition method, we first utilized every tremor burst when  
142 decomposing the GNSS time series without distinguishing whether the burst occurred during or  
143 in between identified deep SSEs. For each tremor cluster, we estimated the corresponding  
144 displacement in the GNSS time series horizontal components by computing the difference  
145 between average positions 10 days after and before each cluster. Displacements and durations of  
146 each tremor cluster were stacked to produce a time series of cumulative displacement increments  
147 for both horizontal components on each station (Figure 2, S3). Similarly, cumulative  
148 displacement increments during the inter-tremor period (i.e., times of no tremor) were measured.  
149 We performed a linear regression to the tremor and inter-tremor displacement time series to find  
150 time-averaged displacement rates (i.e., time-averaged velocities). Tremor and inter-tremor  
151 velocity vectors were plotted to obtain a sense of direction and to confirm that vectors were  
152 spatially coherent (Figure 3a). To find the true tremor velocity, we isolated the tremor signal by  
153 subtracting the inter-tremor velocity from the velocity during the tremor period (Figure 3b).  
154 Essentially, we removed the plate convergence rate, the slip associated with mid- to long-term  
155 SSEs but not associated with times of tremor, and any other long-term signals from the tremor  
156 signal by subtracting out the inter-tremor velocity such that the new tremor velocities were  
157 relative to an ‘inter-tremor motion’ fixed reference. In discussing the results of this study, we  
158 will refer to the true tremor velocities in the ‘inter-tremor motion’ fixed reference frame as

159 simply the ‘tremor velocities’. The uncertainty of the velocities was determined by taking the  
160 standard deviation from the population of velocities generated through random resampling of the  
161 displacement increments.

162 We sought to determine if tremor-associated motions were affected by the deep mid- to  
163 long-term SSEs in the Manawatu and Kaimanawa regions. We computed time-averaged tremor  
164 and inter-tremor velocities only during the mid- to long-term SSEs via decomposition (Figure  
165 S4-S5). The deep SSEs during the time frame analyzed were the 2004-2005, 2010-2011, 2014-  
166 2015 Manawatu SSEs and the 2006, 2008, 2013 Kaimanawa SSEs (Figure S2) (Bartlow et al.,  
167 2014; Wallace, 2020; Wallace & Beavan, 2010; Wallace & Eberhart-Phillips, 2013). Wallace  
168 and Eberhart-Phillips (2013) identified a shallow SSE in February-March 2013, 20 km updip  
169 from the 2006 and 2008 Kaimanawa SSEs. However, there may have also been a deep SSE  
170 during this time similar to the 2006 and 2008 mid-term Kaimanawa SSEs (personal  
171 communication with Laura Wallace). Therefore, we included this probable deep 2013 event as a  
172 SSE during the decomposition. We also computed time-averaged tremor and inter-tremor  
173 velocities during the inter-SSEs periods (Figure S6-S7). In order to quantify the robustness of  
174 these decompositions with regard to background noise levels, we followed the modified  
175 bootstrapping approach of Rousset et al. (2019) (Figures S8-10). See supporting information for  
176 more details on determining robustness of the decompositions.

### 177 **3 Results**

178 The direction of the time-averaged tremor velocities obtained from all clusters for  
179 stations closest to the tremor were spatially coherent and oriented southeast consistent with slip  
180 on the plate interface (Figure 3b). Tremor velocities were negligible at far-field stations and only  
181 significant at stations closest to the Manawatu tremor as we would expect (Figure 3b). This  
182 supports that the decomposition method was able to detect a geodetic signal associated with the  
183 tremor. With the exception of the stations updip of the tremor, the magnitude of the tremor  
184 displacement rates was larger than those during the inter-tremor periods suggesting the plate  
185 interface below stations within and downdip from the tremor was slipping faster than during  
186 times of no tremor. Time-averaged tremor surface displacement rates ranged from 3-7 mm/yr.



187

188 **Figure 3.** Time-averaged displacement rate and slip rate for all tremor bursts. a) Displacement  
 189 rate of tremor (red arrows) and inter-tremor periods (blue arrows) with  $1\sigma$  uncertainties are  
 190 shown. GeoNet GNSS station names are in purple. b) A zoomed out view of true tremor  
 191 displacement rates with the ‘inter-tremor motion’ fixed (yellow arrows) and  $1\sigma$  uncertainty. c)  
 192 Comparison of the true tremor displacement rates (yellow arrows) and modeled tremor  
 193 displacement rates (black arrows). d) Time-averaged slip rate during tremor bursts as estimated  
 194 by static slip inversion.

195 For tremor that occurred during the deep, mid- to long-term Manawatu and Kaimanawa  
196 SSEs, we also saw a coherent signal among stations closest to the tremor with all but two stations  
197 oriented towards the trench (Figure S5). The magnitude of tremor displacement rates were larger  
198 than those when considering the entire tremor catalog suggesting a potential influence of the  
199 deep SSEs. Tremor displacement rates during deep SSEs ranged from 5-10 mm/yr. The tremor  
200 signal was not as spatially coherent for tremor during the inter-SSE period and was very small  
201 (1-4 mm/yr) yet still visible at some stations ( Figure S7). The lack of a spatially coherent tremor  
202 signal during the inter-SSE period is likely a result of the weak robustness of the decomposition  
203 for the inter-SSE period (Figure S10).

### 204 **3.1 Static Slip Inversion**

205 We used a weighted, Laplacian smoothed, nonnegative least squares inversion with  
206 heterogeneous Green's functions to invert the time-averaged tremor velocities (Figure 3) for  
207 tremor-associated slip rate on the plate interface. We used a triangular mesh to represent the fault  
208 surface, using the Hikurangi fault geometry of Williams et al. (2013). We embedded the fault  
209 geometry within a tetrahedral volume mesh and used the finite element code PyLith (Aagaard et  
210 al., 2013, 2017a, 2017b) to generate Green's functions for the observation sites. By using PyLith  
211 to generate our Green's functions, we were able to account for elastic heterogeneity using the  
212 New Zealand-wide seismic velocity model (Eberhart-Phillips et al., 2010; Eberhart-Phillips &  
213 Bannister, 2015; Eberhart-Phillips & Reyners, 2012; Reyners et al., 2014). As shown by  
214 Williams and Wallace (2015, 2018), accounting for elastic heterogeneity typically has a large  
215 effect on slip; for deep events, accounting for elastic heterogeneity decreases estimated slip by  
216 about 20%. Slip direction was specified for each triangle using the tectonic block model of  
217 Wallace, Beavan et al. (2012).

218 Both the data and Green's functions were weighted with the inverse of the tremor velocity  
219 uncertainties. Smoothing was applied by appending a discrete Laplacian matrix onto the Green's  
220 function matrix and zeros to the data vector. The Laplacian matrix was scaled by the Green's  
221 function amplitudes and multiplied by a smoothing parameter of 16, selected by visual inspection  
222 of an L-curve (Figure S11). MATLAB's nonnegative least squares function (lsqnonneg) was  
223 used to impose nonnegativity, preventing reversal of slip of the plate interface. For specifics on  
224 the inversion, see Bartlow (2020). The resulting slip rate estimates should be considered time-

225 averaged estimates of tremor slip rate, which are not applicable to a single tremor cluster. The  
226 time-averaged tremor velocities during SSE and inter-SSE periods were also inverted. We  
227 calculated a total moment rate for each of the three modeled slip rate solutions and estimated the  
228 average moment per tremor burst (Table S1). For details on the moment rate calculation, see the  
229 supplement.

230 Inverting the time-averaged tremor displacement rates considering all tremor clusters  
231 revealed tremor-associated slip co-located with the tremor and in the Manawatu and Kaimanawa  
232 SSE source regions (Figure 3d). Maximum slip rates were 45-50 mm/yr and updip from the  
233 region of tremor, coinciding with the downdip edge of the Kaimanawa SSEs. There was a second  
234 slip rate maximum, ~40 mm/yr, which coincided with the Manawatu SSE source region. Slip  
235 rates in the tremor region were 10-30 mm/yr. The total moment rate for the entire slip area was  
236  $2.4 \times 10^{19}$  Nm/yr, while the average moment per tremor burst was  $1.5 \times 10^{18}$  Nm equivalent to a  
237  $M_W$  5.0.

238 Decomposition for the SSE period revealed periods of fast slip associated with the  
239 tremor. Tremor slip rates during the deep SSEs also showed two maximum slip patches updip  
240 from the region of tremor coinciding with the Kaimanawa (70-80 mm/yr) and Manawatu (~55  
241 mm/yr) SSEs (Figure S5). The maximum tremor slip rate coinciding with the Kaimanawa SSEs  
242 was nearly twice as large during SSEs than when not distinguishing times of SSEs. Slip rates in  
243 the tremor region were 15-40 mm/yr. The total moment rate was  $3.4 \times 10^{19}$  Nm/yr, while the  
244 average moment per tremor burst was  $3.0 \times 10^{18}$  Nm, equivalent to a  $M_W$  5.2.

245 Results from decomposition of the inter-SSE period were less conclusive due to more  
246 stations being less robust. This meant at most stations (9/12 for the east component) the velocity  
247 during tremor could not be distinguished from the inter-tremor period with less than a  $1\sigma$   
248 difference (Figure S10). Since there were still a few stations with at least a  $1\sigma$  difference, we ran  
249 the inversion. Interestingly, the model produced a single slip patch near the tremor source region  
250 (max of ~25 mm/yr) and no slip patch in the Manawatu or Kaimanawa SSE regions, albeit there  
251 was a poor fit with the model (Figure S7). Slip rates in the tremor region were 5-20 mm/yr. The  
252 total moment rate was  $9.4 \times 10^{18}$  Nm/yr, and the average moment per tremor burst was  $4.4 \times 10^{17}$   
253 Nm, equivalent to a  $M_W$  4.6.

#### 254 **4 Small, short-term ETS-like events at deep, central Hikurangi margin**

255 In this study we detected another type of slow slip in this segment of the Hikurangi  
256 margin associated with the deep tremor, which we interpret as ETS-like events, a new  
257 observation of slow slip for the Hikurangi margin. Our findings support the general idea that  
258 seismically observed tectonic tremor can be used to infer the existence of slow slip.

259 The slip inversion indicated slip on the plate interface in the region of tremor, but  
260 maximum slip rates were updip of the tremor and overlapping with the downdip end of the  
261 Kaimanawa and Manawatu SSE source regions. This slip was only detectable when tremor  
262 occurred during mid- to long-term SSEs, implying that the ETS-like slip associated with tremor  
263 is also accompanied by an acceleration of the updip larger SSE. Our data were well-fit with the  
264 assumption that slip occurs on the plate interface, but short-term SSEs on structures other than  
265 the plate interface cannot be ruled out. While we are confident that the decomposition revealed a  
266 geodetic signal associated with the tremor, our ability to interpret the location of slip relative to  
267 the tremor was limited. The location of our model was not well-constrained, and there were  
268 uncertainties with tremor locations such that we cannot rule out that the tremor and short-term  
269 SSEs were indeed co-located. There were a limited number of stations we were able to use up  
270 dip of the tremor as those stations included signals from the shallow east coast SSEs. In addition,  
271 there were no stations directly on top of the tremor due to the terrain in the region nor were there  
272 enough long running stations north of the tremor. Romanet and Ide (2019) noted the relative  
273 location of the tremor may not be accurate as they found a standard deviation of  $0.15^\circ$  longitude  
274 and  $0.12^\circ$  latitude for the difference between their locations of earthquakes and the locations  
275 given by the GeoNet catalog. Even though the exact location of the deep short-term SSEs  
276 relative to the tremor was not fully resolvable at this time, the geodetic signal associated with the  
277 tremor was coherent across several stations near the tremor and negligible at far-field stations  
278 suggesting that this was a real geodetic signal.

279 In seeking to characterize the ETS-like events during versus in between the mid- to long-  
280 term SSEs, we concluded that short-term ETS-like events could robustly be detected during the  
281 mid- to long-term SSEs but those during the inter-SSE periods could not. Decomposition of the  
282 inter-SSE time series indicated all but four stations had tremor velocities less than  $1\sigma$  uncertainty  
283 from the mean velocity generated through random decompositions. We suspect this to be a result  
284 of too small of a SSE to be detected at all stations even through the decomposition method.  
285 However, we speculate that tremor during the inter-SSE periods were occurring with small ETS-

286 like SSEs. Equivalent moment magnitudes of an average tremor burst for each of the three  
287 regimes were a good justification for why we can't detect these small short-term ETS-like SSEs  
288 individually as they are expected to be below the geodetic detection threshold. However, we  
289 demonstrated that decomposition with respect to times of tremor effectively stacks multiple  
290 events and served as a method for identification and estimation of size for ETS-like events below  
291 the geodetic detection threshold.

292 To support the fact that the geodetic signal we observed was not simply the mid- to long-  
293 term SSE signal, decomposition of the time series during the mid- to long-term SSEs showed  
294 displacement rates during tremor were higher than during the SSEs without tremor. Therefore,  
295 mid- to long-term SSEs may influence deep short-term SSEs by increasing slip rates for which  
296 there are two equivalent interpretations. Under one interpretation, faster slip-rates of ETS-like  
297 events during SSEs are driven by the stress shadow effect created by the larger SSEs updip. The  
298 SSE that is updip from the tremor will slip faster relatively, generating a stress shadow downdip  
299 which will increase the shear stress in the source region of the tremor, hence increasing the rate  
300 of tremor failure compared to when mid- to long-term SSEs are not occurring (Frank et al., 2018).  
301 The ETS-like slip in turn will add shear stress to the updip SSE region, accelerating ongoing slip  
302 there, which may explain our observed tremor-associated slip in the updip SSE regions during  
303 the SSE periods (Figure S5). This interpretation is illustrated in Figure 1b. With this  
304 understanding, it makes sense that the inter-SSE periods have smaller tremor-associated slip and  
305 no slip in the mid- to long-term SSE zones, albeit these results were not robust. Alternatively, we  
306 can interpret that the mid- to long-term SSEs merely fluctuate and move in and out of the tremor-  
307 generating region, generating tremor only when they enter this region, which tends to be when  
308 the slip rate is higher in the adjacent updip region. These interpretations can be seen as  
309 essentially equivalent during the mid- to long-term SSEs. However, we interpret the occurrence  
310 of tremor outside the times of mid- to long-term SSEs as evidence for the first interpretation.

## 311 **5 Conclusions**

312 This study identified and modeled a geodetic signal associated with deep tectonic tremor.  
313 We found the plate interface below the deep mid- to long-term SSEs in Manawatu and  
314 Kaimanawa regions may slip often, in small, short-term SSEs with tremor, which we refer to as  
315 ETS-like (Figure 1b). This is a new observation of slow slip behavior in New Zealand which

316 implies that there are three types of slow slip that overlap along-strike, 1) shallow, short-term  
317 SSEs, 2) deep, mid- to long-term SSEs, and 3) deeper, short-term ETS-like SSEs with tremor. In  
318 addition, the mid- to long-term SSEs may influence the deep, short-term ETS-like events by  
319 increasing slip rates, and the ETS-like events in turn may increase slip rates in mid-to-long term  
320 SSEs. Similar observations of deep, small, short-term SSEs co-located with tremor and long-  
321 term SSEs located updip from tremor have been observed in Japan, Mexico and Alaska (Frank et  
322 al., 2018; Hirose & Obara, 2005; Hirose et al., 2010; Rousset et al., 2019). However, the  
323 Hikurangi margin also has shallow, short-term SSEs which may be separated from the region of  
324 mid- to long-term SSEs by a region of creeping (Wallace, 2020). The nature of the strong  
325 variabilities in SSE depths and durations in the central Hikurangi margin is still not well  
326 understood.

327         The decomposition method relies on a catalog of tremor to ensure proper identification of  
328 start and end times of tremor bursts which are subsequently used for measuring displacement  
329 increments and tremor-associated velocities. Tremor is difficult to detect in New Zealand as the  
330 high rates of seismicity make automatic detection and location of tremor challenging, and we  
331 expect that the tremor catalog is incomplete (Romanet & Ide, 2019). We do not know if tremor  
332 bursts were missed or if apparent durations are a mis-representation of the true duration due to  
333 too few events able to be detected. Therefore, the tremor catalog is one caveat to this method and  
334 results from this study are meant to be an estimation of average tremor velocities and slip rates.  
335 As network coverage, tremor detection methods, and detection of low-frequency earthquakes  
336 improve in New Zealand, the spatiotemporal relationship between deep, ETS-like events and  
337 mid- to long-term SSEs can be better understood.

### 338 **Acknowledgments**

339 This work was supported by departmental funds from the University of Kansas Geology  
340 Department. The authors thank Dr. Laura Wallace for her insightful discussions which benefited  
341 this study. The authors also thank graphic designer Hailey Stepanek for helping make Figure 1b.

### 342 **Data Availability Statement**

343 Daily time-series solutions from continuous GNSS stations can be obtained from the GeoNet  
344 Aotearoa New Zealand Continuous GNSS Network (<https://doi.org/10.21420/30F4-1A55>).

345 Timing of the offsets were obtained from the University of Nevada-Reno steps database  
346 (<http://geodesy.unr.edu/NGLStationPages/steps.txt>). The tectonic tremor catalog from Romanet  
347 and Ide (2019) is available via <https://doi.org/10.1186/s40623-019-1039-1>

## 348 References

- 349 Aagaard, B. T., Knepley, M. G., & Williams, C. A. (2013). A domain decomposition approach to  
350 implementing fault slip in finite-element models of quasi-static and dynamic crustal  
351 deformation. *Journal of Geophysical Research Solid Earth*, 118, 3059–3079.  
352 <https://doi.org/10.1002/jgrb.50217>
- 353 Aagaard, B. T., Knepley, M. G., & Williams, C. A. (2017a). PyLith v2.2.1, Computational  
354 Infrastructure for Geodynamics. <https://doi.org/10.5281/zenodo.886600>, Retrieved from  
355 <https://geodynamics.org/cig/software/pylith/>
- 356 Aagaard, B. T., Knepley, M. G., & Williams, C. A. (2017b). PyLith user manual, version 2.2.0,  
357 Computational Infrastructure for Geodynamics, Davis, CA. Retrieved from  
358 [https://geodynamics.org/cig/software/github/pylith/v2.2.0/pylith-2.2.0\\_manual.pdf](https://geodynamics.org/cig/software/github/pylith/v2.2.0/pylith-2.2.0_manual.pdf)
- 359 Altamimi, Z., Métivier, L., & Collilieux, X. (2012). ITRF2008 plate motion model. *Journal of*  
360 *Geophysical Research: Solid Earth*, 117(B7). <https://doi.org/10.1029/2011JB008930>
- 361 Bartlow, N. M. (2020). A long-term view of episodic tremor and slip in Cascadia. *Geophysical*  
362 *Research Letters*, 47(3), e2019GL085303. <https://doi.org/10.1029/2019GL085303>
- 363 Bartlow, N. M., Miyazaki, S. I., Bradley, A. M., & Segall, P. (2011). Space-time correlation of  
364 slip and tremor during the 2009 Cascadia slow slip event. *Geophysical Research Letters*,  
365 38(18). <https://doi.org/10.1029/2011GL048714>
- 366 Bartlow, N. M., Wallace, L. M., Beavan, R. J., Bannister, S., & Segall, P. (2014). Time-  
367 dependent modeling of slow slip events and associated seismicity and tremor at the  
368 Hikurangi subduction zone, New Zealand. *Journal of Geophysical Research: Solid Earth*,  
369 119(1), 734–753. <https://doi.org/10.1002/2013JB010609>
- 370 Beavan, J., Tregoning, P., Bevis, M., Kato, T., & Meertens, C. (2002). Motion and rigidity of the  
371 Pacific Plate and implications for plate boundary deformation. *Journal of Geophysical*  
372 *Research: Solid Earth*, 107(B10), ETG-19. <https://doi.org/10.1029/2001JB000282>

- 373 Beroza, G. C., & Ide, S. (2011). Slow earthquakes and nonvolcanic tremor. *Annual review of*  
374 *Earth and planetary sciences*, 39, 271–296. [https://doi.org/10.1146/annurev-earth-040809-](https://doi.org/10.1146/annurev-earth-040809-152531)  
375 [152531](https://doi.org/10.1146/annurev-earth-040809-152531)
- 376 Brown, J. R., Beroza, G. C., Ide, S., Ohta, K., Shelly, D. R., Schwartz, S. Y., et al. (2009). Deep  
377 low-frequency earthquakes in tremor localize to the plate interface in multiple subduction  
378 zones. *Geophysical Research Letters*, 36(19). <https://doi.org/10.1029/2009GL040027>
- 379 Delahaye, E. J., Townend, J., Reyners, M. E., & Rogers, G. (2009). Microseismicity but no  
380 tremor accompanying slow slip in the Hikurangi subduction zone, New Zealand. *Earth and*  
381 *Planetary Science Letters*, 277(1-2), 21–28. <https://doi.org/10.1016/j.epsl.2008.09.038>
- 382 Dragert, H., Wang, K., & James, T. S. (2001). A silent slip event on the deeper Cascadia  
383 subduction interface. *Science*, 292(5521), 1525–1528.  
384 <https://doi.org/10.1126/science.1060152>
- 385 Eberhart-Phillips, D., & Bannister, S. (2015). 3-D imaging of the northern Hikurangi subduction  
386 zone, New Zealand: Variations in subducted sediment, slab fluids and slow slip.  
387 *Geophysical Journal International*, 201(2), 838–855. <https://doi.org/10.1093/gji/ggv057>
- 388 Eberhart-Phillips, D., & Reyners, M. (2012). Imaging the Hikurangi plate interface region with  
389 improved local-earthquake tomography. *Geophysical Journal International*, 190(2), 1221–  
390 1242. <https://doi.org/10.1111/j.1365-246X.2012.05553.x>
- 391 Eberhart-Phillips, D., Reyners, M., Bannister, S., Chadwick, M., & Ellis, S. (2010). Establishing  
392 a versatile 3-D seismic velocity model for New Zealand. *Seismological Research Letters*,  
393 81(6), 992–1000. <https://doi.org/10.1785/gssrl.81.6.992>
- 394 Frank, W. B., Rousset, B., Lasserre, C., & Campillo, M. (2018). Revealing the cluster of slow  
395 transients behind a large slow slip event. *Science advances*, 4(5), eaat0661.  
396 <https://doi.org/10.1126/sciadv.aat0661>
- 397 Gao, X., & Wang, K. (2017). Rheological separation of the megathrust seismogenic zone and  
398 episodic tremor and slip. *Nature*, 543(7645), 416–419. <https://doi.org/10.1038/nature21389>
- 399 GNS Science. (2000). GeoNet Aotearoa New Zealand Continuous GNSS Network Time Series  
400 Dataset [Data set]. GNS Science, GeoNet. <https://doi.org/10.21420/30F4-1A55>
- 401 Graham, S. E., DeMets, C., Cabral-Cano, E., Kostoglodov, V., Walpersdorf, A., Cotte, N., et al.,  
402 (2014). GPS constraints on the 2011–2012 Oaxaca slow slip event that preceded the 2012

- 403 March 20 Ometepec earthquake, southern Mexico. *Geophysical Journal International*,  
404 197(3), 1593–1607. <https://doi.org/10.1093/gji/ggu019>
- 405 Hawthorne, J. C., & Rubin, A. M. (2013). Short-time scale correlation between slow slip and  
406 tremor in Cascadia. *Journal of Geophysical Research: Solid Earth*, 118(3), 1316–1329.  
407 <https://doi.org/10.1002/jgrb.50103>
- 408 Hirose, H., Y. Asano, K. Obara, T. Kimura, T. Matsuzawa, S. Tanaka, and T. Maeda (2010).  
409 Slow earthquakes linked along dip in the Nankai subduction zone. *Science*, 330, 1502.  
410 <https://doi.org/10.1126/science.1197102>
- 411 Hirose, H., & Obara, K. (2005). Repeating short-and long-term slow slip events with deep tremor  
412 activity around the Bungo channel region, southwest Japan. *Earth, planets and space*,  
413 57(10), 961–972. <https://doi.org/10.1186/BF03351875>
- 414 Hyndman, R. D., McCrory, P. A., Wech, A., Kao, H., & Ague, J. (2015). Cascadia subducting  
415 plate fluids channelled to fore-arc mantle corner: ETS and silica deposition. *Journal of*  
416 *Geophysical Research: Solid Earth*, 120(6), 4344–4358.  
417 <https://doi.org/10.1002/2015JB011920>
- 418 Ide, S., Shelly, D. R., & Beroza, G. C. (2007). Mechanism of deep low frequency earthquakes:  
419 Further evidence that deep non-volcanic tremor is generated by shear slip on the plate  
420 interface. *Geophysical Research Letters*, 34(3). <https://doi.org/10.1029/2006GL028890>
- 421 Jacobs, K. M., Savage, M. K., & Smith, E. C. G. (2016). Quantifying seismicity associated with  
422 slow slip events in the Hikurangi margin, New Zealand. *New Zealand Journal of Geology*  
423 *and Geophysics*, 59(1), 58–69. <https://doi.org/10.1080/00288306.2015.1127827>
- 424 Kato, A., Obara, K., Igarashi, T., Tsuruoka, H., Nakagawa, S., & Hirata, N. (2012). Propagation  
425 of slow slip leading up to the 2011 Mw 9.0 Tohoku-Oki earthquake. *Science*, 335(6069),  
426 705–708. <https://doi.org/10.1126/science.1215141>.
- 427 Langridge, R. M., Ries, W. F., Litchfield, N. J., Villamor, P., Van Dissen, R. J., Barrell, D. J. A.,  
428 et al., (2016). The New Zealand Active Faults Database. *New Zealand Journal of Geology*  
429 *and Geophysics*, 59, 86–96. <https://doi.org/10.1080/00288306.2015.1112818>
- 430 Obara, K. (2002). Nonvolcanic deep tremor associated with subduction in southwest Japan.  
431 *Science*, 296(5573), 1679–1681. <https://doi.org/10.1126/science.1070378>

- 432 Obara, K., Hirose, H., Yamamizu, F., & Kasahara, K. (2004). Episodic slow slip events  
433 accompanied by non-volcanic tremors in southwest Japan subduction zone. *Geophysical*  
434 *Research Letters*, 31(23). <https://doi.org/10.1029/2004GL020848>
- 435 Obara, K., & Kato, A. (2016). Connecting slow earthquakes to huge earthquakes. *Science*,  
436 353(6296), 253–257. <https://doi.org/10.1126/science.aaf1512>
- 437 Radiguet, M., Cotton, F., Vergnolle, M., Campillo, M., Walpersdorf, A., Cotte, N., &  
438 Kostoglodov, V. (2012). Slow slip events and strain accumulation in the Guerrero gap,  
439 Mexico. *Journal of Geophysical Research: Solid Earth*, 117(B4).  
440 <https://doi.org/10.1029/2011JB008801>
- 441 Radiguet, M., Perfettini, H., Cotte, N., Gualandi, A., Valette, B., Kostoglodov, V., et al. (2016).  
442 Triggering of the 2014 M w 7.3 Papanoa earthquake by a slow slip event in Guerrero,  
443 Mexico. *Nature Geoscience*, 9(11), 829–833. <https://doi.org/10.1038/ngeo2817>
- 444 Reyners, M., & Bannister, S. (2007). Earthquakes triggered by slow slip at the plate interface in  
445 the Hikurangi subduction zone, New Zealand. *Geophysical research letters*, 34(14).  
446 <https://doi.org/10.1029/2007GL030511>
- 447 Reyners, M., Eberhart-Phillips, D., & Martin, S. (2014). Prolonged Canterbury earthquake  
448 sequence linked to widespread weakening of strong crust. *Nature Geoscience*, 7(1), 34–37.  
449 <https://doi.org/10.1038/ngeo2013>
- 450 Rogers, G., & Dragert, H. (2003). Episodic tremor and slip on the Cascadia subduction zone:  
451 The chatter of silent slip. *Science*, 300(5627), 1942–1943.  
452 <https://doi.org/10.1126/science.1084783>
- 453 Romanet, P., & Ide, S. (2019). Ambient tectonic tremors in manawatu, Cape Turnagain,  
454 marlborough, and Puysegur, New Zealand. *Earth, Planets and Space*, 71(1), 1–9.  
455 <https://doi.org/10.1186/s40623-019-1039-1>
- 456 Rousset, B., Fu, Y., Bartlow, N., & Bürgmann, R. (2019). Weeks-long and years-long slow slip  
457 and tectonic tremor episodes on the south central Alaska Megathrust. *Journal of*  
458 *Geophysical Research: Solid Earth*, 124(12), 13392–13403.  
459 <https://doi.org/10.1029/2019JB018724>
- 460 Ruiz, S., Metois, M., Fuenzalida, A., Ruiz, J., Leyton, F., Grandin, R., et al., (2014). Intense  
461 foreshocks and a slow slip event preceded the 2014 Iquique M w 8.1 earthquake. *Science*,  
462 345(6201), 1165–1169. <https://doi.org/10.1126/science.1256074>

- 463 Shaddox, H. R., & Schwartz, S. Y. (2019). Subducted seamount diverts shallow slow slip to the  
464 forearc of the northern Hikurangi subduction zone, New Zealand. *Geology*, 47(5), 415–418.  
465 <https://doi.org/10.1130/G45810.1>
- 466 Shelly, D. R., Beroza, G. C., & Ide, S. (2007). Non-volcanic tremor and low-frequency  
467 earthquake swarms. *Nature*, 446(7133), 305–307. <https://doi.org/10.1038/nature05666>
- 468 Shelly, D. R., Beroza, G. C., Ide, S., & Nakamura, S. (2006). Low-frequency earthquakes in  
469 Shikoku, Japan, and their relationship to episodic tremor and slip. *Nature*, 442(7099), 188–  
470 191. <https://doi.org/10.1038/nature04931>
- 471 Todd, E. K., & Schwartz, S. Y. (2016). Tectonic tremor along the northern Hikurangi Margin,  
472 New Zealand, between 2010 and 2015. *Journal of Geophysical Research: Solid Earth*,  
473 121(12), 8706–8719. <https://doi.org/10.1002/2016JB013480>
- 474 Todd, E. K., Schwartz, S. Y., Mochizuki, K., Wallace, L. M., Sheehan, A. F., Webb, S. C., et al.  
475 (2018). Earthquakes and tremor linked to seamount subduction during shallow slow slip at  
476 the Hikurangi margin, New Zealand. *Journal of Geophysical Research: Solid Earth*, 123(8),  
477 6769–6783. <https://doi.org/10.1029/2018JB016136>
- 478 Villafuerte, C., & Cruz-Atienza, V. M. (2017). Insights into the causal relationship between slow  
479 slip and tectonic tremor in Guerrero, Mexico. *Journal of Geophysical Research: Solid*  
480 *Earth*, 122(8), 6642–6656. <https://doi.org/10.1002/2017JB014037>
- 481 Wallace, L. M. (2020). Slow slip events in New Zealand. *Annual Review of Earth and Planetary*  
482 *Sciences*, 48, 175–203. <https://doi.org/10.1146/annurev-earth-071719-055104>
- 483 Wallace, L. M., Barnes, P., Beavan, J., Van Dissen, R., Litchfield, N., Mountjoy, J., et al. (2012).  
484 The kinematics of a transition from subduction to strike-slip: An example from the central  
485 New Zealand plate boundary. *Journal of Geophysical Research: Solid Earth*, 117(B2).  
486 <https://doi.org/10.1029/2011JB008640>
- 487 Wallace, L. M., & Beavan, J. (2010). Diverse slow slip behavior at the Hikurangi subduction  
488 margin, New Zealand. *Journal of Geophysical Research: Solid Earth*,  
489 115(B12). <https://doi.org/10.1029/2010JB007717>
- 490 Wallace, L. M., Beavan, J., Bannister, S., & Williams, C. (2012). Simultaneous long-term and  
491 short-term slow slip events at the Hikurangi subduction margin, New Zealand: Implications  
492 for processes that control slow slip event occurrence, duration, and migration. *Journal of*  
493 *Geophysical Research: Solid Earth*, 117(B11). <https://doi.org/10.1029/2012JB009489>

- 494 Wallace, L. M., & Eberhart-Phillips, D. (2013). Newly observed, deep slow slip events at the  
495 central Hikurangi margin, New Zealand: Implications for downdip variability of slow slip  
496 and tremor, and relationship to seismic structure. *Geophysical Research Letters*, *40*(20),  
497 5393–5398. <https://doi.org/10.1002/2013GL057682>
- 498 Wech, A. G., & Creager, K. C. (2007). Cascadia tremor polarization evidence for plate interface  
499 slip. *Geophysical Research Letters*, *34*(22). <https://doi.org/10.1029/2007GL031167>
- 500 Williams, C. A., Eberhart-Phillips, D., Bannister, S., Barker, D. H. N., Henrys, S., Reyners, M.,  
501 & Sutherland, R. (2013). Revised interface geometry for the Hikurangi subduction zone,  
502 New Zealand. *Seismological Research Letters*, *84*(6), 1066–1073.  
503 <https://doi.org/10.1785/0220130035>
- 504 Williams, C. A., & Wallace, L. M. (2015). Effects of material property variations on slip  
505 estimates for subduction interface slow-slip events. *Geophysical Research Letters*, *42*(4),  
506 1113–1121. <https://doi.org/10.1002/2014GL062505>
- 507 Williams, C. A., & Wallace, L. M. (2018). The impact of realistic elastic properties on inversions  
508 of shallow subduction interface slow slip events using seafloor geodetic data. *Geophysical  
509 Research Letters*, *45*, 7462–7470. <https://doi.org/10.1029/2018GL078042>
- 510 Wu, Z. L., & Chen, Y. T. (2003). Definition of seismic moment at a discontinuity interface.  
511 *Bulletin of the Seismological Society of America*, *93*(4), 1832–1834.  
512 <https://doi.org/10.1785/0120020234>
- 513 Yabe, S., Ide, S., & Yoshioka, S. (2014). Along-strike variations in temperature and tectonic  
514 tremor activity along the Hikurangi subduction zone, New Zealand. *Earth, Planets and  
515 Space*, *66*, 1–15. <https://doi.org/10.1186/s40623-014-0142-6>
- 516 Yarce, J., Sheehan, A. F., Nakai, J. S., Schwartz, S. Y., Mochizuki, K., Savage, M. K., et al.  
517 (2019). Seismicity at the northern Hikurangi Margin, New Zealand, and investigation of the  
518 potential spatial and temporal relationships with a shallow slow slip event. *Journal of  
519 Geophysical Research: Solid Earth*, *124*(5), 4751–4766.  
520 <https://doi.org/10.1029/2018JB017211>